ELECTRIC IMPEDANCE IMAGING

The imaging of electrical conductivity and permittivity of the interior of a body from fixed-frequency electrical measurements at the boundary has come to be called electrical impedance tomography (EIT) although it is quite different from the true tomographic imaging methods in that slices cannot be imaged independently. The earliest specific references are Langer (1) and Slichter (2) in 1933, but little work was published until Henderson and Webster's paper entitled "An Impedance Camera for Spatially Specific Measurements of the Thorax" (3) in 1979, which proposed EIT as a safe, noninvasive imaging method and stimulated interest in the subject. By this time it was practical (economic) to implement electronic systems capable of measuring with sufficient accuracy and of computing with sufficient speed for use in medical imaging applications. The developments in this context led others to pursue the method, notably in process monitoring and geophysical prospecting, where there are different timescales and boundary constraints.

The method has potential for imaging because of the impedance differences of naturally occurring substances. For example, in the medical context

Resistivity, in $\Omega \cdot m$	
Human blood	1.5
Lung tissue	7.3–24.0
Bone	170
Muscle (longitudinal)	1.3–1.5
Muscle (transverse)	18–23
Brain (gray matter)	2.8
Brain (white matter)	6.8
Fat	21–28
Liver	3.5–5.5

Permittivity is measured when investigating low conductivity substances like air/oil/water mixtures in pipelines by using capacitively coupled electrode systems. Resistive values are typically found when low-frequency excitation is used with directly coupled electrodes on conductive objects. Many of the resistive substances also have a small reactance that becomes measurable when high-frequency excitation is used.

PHYSICAL THEORY

Take a body Ω in three-dimensional space with spatial variable $\boldsymbol{x} = (x, y, z)$ outward unit normal n. Suppose the body has possibly inhomogeneous isotropic conductivity $\sigma(x)$, permittivity $\epsilon(x)$, and permeability $\mu(x)$. A time-harmonic current density $\tilde{\boldsymbol{J}}(x, t) = \boldsymbol{J}(x)e^{-j\omega t}$ with angular frequency ω is applied to the surface $\partial\Omega$, and this results after some settling time in an electric field $\tilde{\boldsymbol{E}}(x, t) = \boldsymbol{E}(x)e^{-j\omega t}$ and magnetic field $\tilde{\boldsymbol{H}}(x, t) = \boldsymbol{H}(x)e^{-j\omega t}$ in the body. Maxwell's equations then give us

$$\nabla \times \boldsymbol{E} = j\omega\mu\boldsymbol{H}$$
$$\nabla \times \boldsymbol{H} = (\sigma - j\omega\epsilon)\boldsymbol{E} \quad (1)$$

Assuming sufficiently small permeability and frequency, we make the approximation $\nabla \times \boldsymbol{E} = 0$ and therefore $\boldsymbol{E} = \nabla\phi$, where ϕ is the electric potential. We now define the complex conductivity or admittivity $\gamma = \sigma - j\omega\epsilon$ and we have the partial differential equation

$$\nabla \cdot (\gamma\nabla\phi) = \frac{\partial}{\partial x}\left(\gamma\frac{\partial\phi}{\partial x}\right) + \frac{\partial}{\partial y}\left(\gamma\frac{\partial\phi}{\partial y}\right) + \frac{\partial}{\partial z}\left(\gamma\frac{\partial\phi}{\partial z}\right) = 0 \quad (2)$$

(which is the continuum equivalent of Ohm's law and Kirchhoff's law combined) subject to the Neumann boundary condition

$$\boldsymbol{n} \cdot \gamma\nabla\phi|_{\partial\Omega} = \boldsymbol{J} \quad (3)$$

For a known admittivity, solving the boundary value problem given by Eqs. (2) and (3) will be called the forward problem. It can be solved numerically using, for example, the finite element method (FEM). In EIT one applies a number of independent current patterns $\boldsymbol{J}$ at the surface and makes measurements of the potential $\phi|_{\partial\Omega}$ also at the surface in an attempt to determine γ in the interior. This is called the inverse problem.

Once the current density on the boundary and the admittivity is specified, the potential is determined up to an additive constant, which we eliminate by setting

$$\int_{\partial\Omega} \phi \, dS = 0$$

As there are no sources of current in the interior, Gauss's law implies that the surface integral of the current density vanishes

$$\int_{\partial\Omega} J dS = 0$$

With these conditions surface current density and surface potential are related by a linear operator, the transfer impedance operator $R(\gamma)J = \phi|_{\partial\Omega}$ (referred to in the mathematical literature as the Neumann-to-Dirichlet mapping). The operator $R(\gamma)$ represents a complete knowledge of boundary electrical data. In EIT we sample this operator using a system of electrodes to apply current and measure potential.

The first problem that needs to be addressed is the theoretical possibility of determining γ from $R(\gamma)$. Specifically, the question "Does $R(\gamma_1) = R(\gamma_2)$ imply $\gamma_1 = \gamma_2$?" has been answered in the affirmative under a variety of smoothness assumptions for the γ_i. For details of these results, including the case where the γ_i are complex, see Isakov (4). The closely related problem of recovering the resistance values of a planar resistor network by boundary current and voltage measurement has been investigated by Curtis and Morrow (5) and Colin de Verdiere (6).

For the case where $\omega\mu$ is not negligible, Ola and Somersalo (7) show that the electrical parameters γ and μ are uniquely determined by a complete knowledge of boundary data $n \times E|_{\partial\Omega}$ and $n \times H|_{\partial\Omega}$, provided ω is not the resonant frequency.

The problem of actually recovering the admittivity from a noisy, sampled boundary data is difficult for two main reasons: The problem is nonlinear and ill posed. Notice that the potential ϕ depends on γ, so that Eq. (2) is a nonlinear equa-

tion for ϕ as a function of γ. The nonlinearity is illustrated for a simple but typical example in Fig. 1.

The current is applied to the surface and voltage measurements made using a system of conducting electrodes. A typical EIT system with l drive electrodes $D_1, \ldots, D_l$ and m measurement electrodes $M_1, \ldots, M_m$ will have single-ended digitally controlled current sources connected to all but one drive electrode (multiple-drive system), or a single double-ended current source connected to the drive electrodes by a system of multiplexers (pair drive system). The in phase and quadrature components of the voltage are measured each of the measurement electrodes.

A current pattern takes the form $J_i = I_{i1}\chi_1 + \cdots + I_{il}\chi_l$, where χ_j is the normalized current density on the jth drive electrode (which for the moment we will assume to be one on the electrode and zero elsewhere), assuming the area of each drive electrode is the same $I_1 + \cdots + I_l = 0$. Let us assume for simplicity that measurement electrodes are points and that voltage is measured relative to M_m. Let ϕ_j be the potential when J_j is applied. Then the measurements made are

$$V_{ij} = \phi_j(M_i) - \phi_j(M_m) = \int_{\partial\Omega} \phi_j(\boldsymbol{x})(\delta(\boldsymbol{x} - M_i) - \delta(\boldsymbol{x} - M_m))\, dS \tag{4}$$

We define the lead field ψ_i to be the potential that would arise if a unit current were passed through the *measurement* elec-

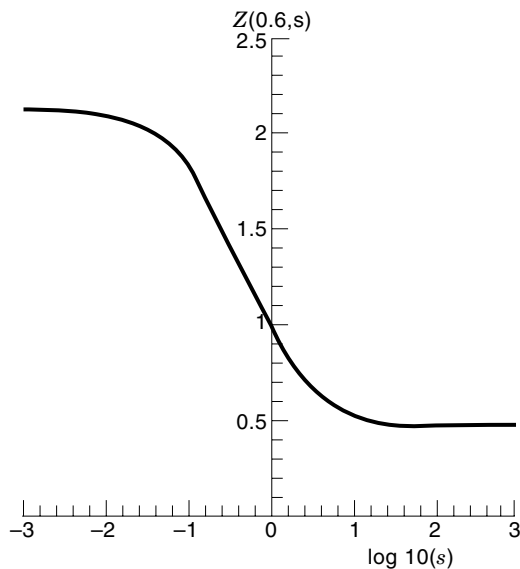**Figure 1.** The simple example illustrates the typical sigmoid response of boundary impedance measurement to interior conductivity change. Let Ω be a unit height unit radius cylinder. Suppose that the current density on the surface (using cylindrical coordinates (ρ, θ, z) is $J(1, \theta, z) = \cos\theta$ and $J(\rho, \theta, \pm 1/2) = 0$. Let us assume a cylindrical anomaly with radius r and conductivity

$$\gamma(\rho, \theta, z) = \begin{cases} 1 & r < \rho \leq 1 \\ s & 0 \leq \rho \leq r \end{cases}$$

Then $\phi(1, \theta, z) = Z(s, r)\cos\theta$, where $Z(s, r) = 1 - mr^2/1 + mr^2$ and $m = (s - 1)/(s + 1)$. The figure illustrates the response of the boundary impedance Z to a change in conductivity contrast over six decades for a radius of 0.6.
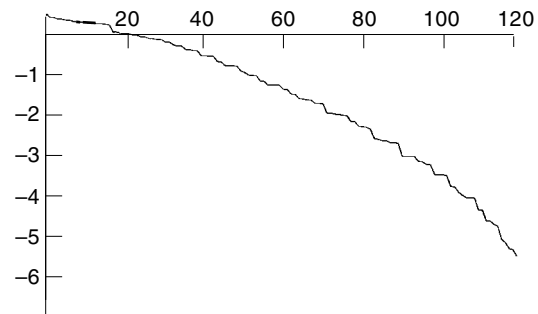
Figure 2. The singular values of the sensitivity matrix give a clear illustration of ill conditioning of the linearized inverse problem. The singular values of $\boldsymbol{S}$ are the square roots of the eigenvalues of $\boldsymbol{S}^T\boldsymbol{S}$ arranged as a decreasing sequence $\lambda_1 \geq \lambda_2 \geq \Lambda \geq 0$. For a signal-to-noise ratio of S one would expect to be able to identify K conductivity parameters, where K is the largest integer with $\lambda_1/\lambda_K < S$. These singular values were calculated using a two-dimensional finite element mesh, 16-point electrodes equally spaced, and trigonometric current patterns. [After Breckon (11).]

trodes, $\gamma\partial\psi_i/\partial\boldsymbol{n} = \delta(\boldsymbol{x} - M_i) - \delta(\boldsymbol{x} - M_m)$. We can express the voltage measurement in an integral form as

$$V_{ij} = \int_{\partial\Omega} \phi_j\gamma\partial\psi_i/\partial\boldsymbol{n}\, dS = \int_\Omega \gamma\nabla\psi_i \cdot \nabla\phi_j\, dV \tag{5}$$

RECONSTRUCTION ALGORITHMS

Now suppose that the admittivity is changed to $\gamma + \delta\gamma$ and the potential and lead fields change to $\phi_j + \delta\phi_j$ and $\psi_i + \delta\psi_i$, respectively, while the boundary current densities remain fixed. We then have the expansion

$$\delta V_{ij} = \int_{\partial\Omega} \delta\phi_j\gamma\partial\psi_i/\partial\boldsymbol{n}\, dS = -\int_\Omega \delta\gamma\nabla\psi_i \cdot \nabla\phi_j\, dV$$
$$+ \text{ higher order terms} \tag{6}$$

This gives the basis of a linear reconstruction algorithm. We use a numerical model (FEM, for example) of the system with admittivity γ^m, which can be used to calculate predicted voltages V_{ij}^m. We measure experimental voltages V_{ij}^e and set $\delta V_{ij} = V_{ij}^e - V_{ij}^m$, ignoring the higher-order terms. We can calculate a correction by solving a system $(m - 1)(l - 1)$ integral equations. This system of equations can be written matrix form as $\boldsymbol{V} = \boldsymbol{Sg}$, where $\boldsymbol{V}$ is the vector composed of the δV_{ij} and $\boldsymbol{g}$ is the vector of components of $\delta\gamma$ with respect to some family of independent functions $\Gamma_k(\boldsymbol{x})$, $\delta\gamma(\boldsymbol{x}) = \sum_{k=1}^K g_k\Gamma_k(\boldsymbol{x})$. Typically, a pixel basis is used where each Γ_k is one in the kth pixel (or voxel) and zero elsewhere, but other choices of basis are possible. The Jacobian or sensitivity matrix S then has elements

$$S_{ijk} = \int_\Omega \Gamma_k\nabla\psi_i \cdot \nabla\phi_j\, dV \tag{7}$$

The linear system $\boldsymbol{V} = \boldsymbol{Sg}$ is highly ill conditioned (see Fig. 2), which means that it can only be solved with some regularization or smoothing of the admittivity. A simple example (Tichonov regularization) is to solve instead the system $\boldsymbol{S}^T\boldsymbol{V} = (\boldsymbol{S}^T\boldsymbol{S} + \epsilon^2\boldsymbol{I})\boldsymbol{g}$ for some small parameter ϵ. The resulting conductivity update $\delta\gamma$ can be added to an assumed background

admittivity to produce an approximate image. This simple linear reconstruction algorithm is similar to the NOSER algorithm used by Rensselaer Polytechnic Institute (RPI) (8). As the inverse of $S^TS + \epsilon^2I$ can be precomputed assuming a suitable background conductivity, the algorithm is quite fast (quadratic in the number of measurements used). However, as it is a linear approximation the admittivity contrast will be underestimated and some detail lost (see Fig. 1). A fully nonlinear algorithm can be implemented by recalculating the Jacobian using the updated admittivity and solving the regularized linear system to produce successive updates to the admittivity until the numerical model fits the measured data to within measurement precision. This requires an accurate forward model, including the shape of the domain (8,9) and modeling of the electrode boundary conditions (10). The nonlinear algorithm is more computationally expensive as at each iteration the voltages have to be recalculated and the linear system solved.

There is still debate about the ideal current patterns J_i to drive. For a given constraint on the allowable current levels, an optimal set of current drives can be calculated. In the case where the total dissipated power is the active constraint, the optimal currents are as described by Cheney (12). In the case of a two-dimensional disk where the unknown conductivity is rotationally symmetric, these are the trigonometric current patterns $I_{ik} = \cos i\theta_k$, where θ_k is an angular coordinate of the kth drive electrode and $1 \le i < l/2$ (similar for sine). If the active constraint is the total injected current, only pairs of electrodes should be driven (13); on the other hand, if the maximum current on each electrode is the only constraint, then all electrodes should be driven with positive or negative currents (Walsh functions). In medical applications the belief that limiting the dissipated power is the most important safety criterion has led to the design of systems with multiple current drives.

TISSUE IMPEDANCE

Spectral information is of particular interest in medical applications, where it can improve tissue characterization. A variety of electrical models of tissue have been proposed to explain the variation of impedance with frequency, the most widely used being the Cole plot. The tissue model in Fig. 3 would give rise to the Cole plot in Fig. 4. The difference between the model and experimental findings is explained by assuming that the capacitive element has a complex reactance given by $K(j\omega)^{-a}$, where $\alpha = 1$ would be a standard capacitor, but in tissue $\alpha = 0.8$ typically. A different interpre-
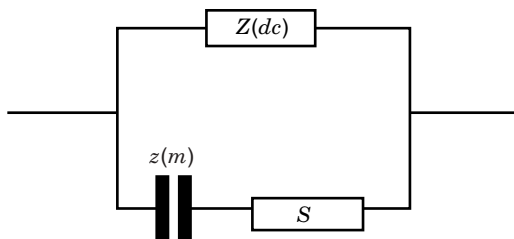

Figure 3. Simplest tissue impedance model where $Z(m)$ is the cell membrane capacitance, S is the intracellular impedance, and $Z(dc)$ is extracellular impedance.
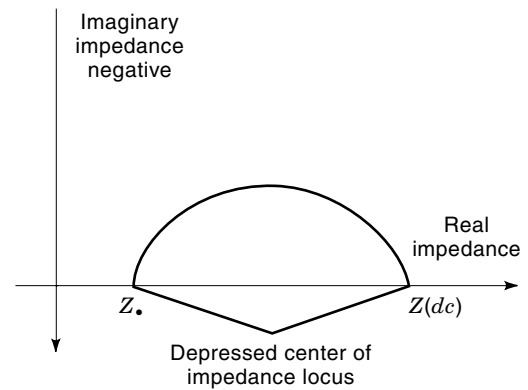

Figure 4. Locus of impedance versus frequency for the simple tissue model.

tation of tissue impedance is that the capacitance is distributed, and this may give a similarly depressed Cole plot. A comprehensive treatment is given in a review by Rigaud (14).

ELECTRONIC SYSTEMS

In any application, the impedance contrast in the region, the size of the smallest distinguishable object, and the rate of change of any impedance in the whole region set the measurement parameters for the electronic and computation tasks.

The majority of systems apply current and measure voltage, and, as the analysis shows, accurate current sources are required in multiple-source systems. Single-current drive systems only require measurement of the current, and no adjustments will be required as long as the current stays constant for the duration of a measurement set. This will be achieved if the output impedance is much larger than the changes in the impedance of the region being imaged. Multiple-drive systems may include current measurement and subsequent adjustment to generate a particular current field, but greater operating speed is possible with deterministic current sources.

High-output impedance current sources have been adapted or developed for EIT in a number of ways. The RPI group uses digitally adjustable negative resistance and negative capacitance circuits on each current source to obtain 64 MΩ (15).

The Oxford Brookes University group uses modified Howland sources to obtain 300 kΩ at 160 kHz (Fig. 5). A calibration system is used to measure the output characteristics and compensate the set current level for each source, thereby allowing very precise currents to be set for as long as the calibration coefficients remain constant.

Alternating currents (ac) are used for several reasons: dc applied to the skin causes electrolytic action under the electrode and may result in ulcers. The maximum ac current that may safely be applied is frequency dependent, with the maximum safe current increasing linearly with frequency between 1 kHz and 100 kHz. Since voltage data accuracy improves with larger applied currents, this implies that the use of higher frequencies may result in more accurate data. However, the accuracy of the data acquisition system may become degraded at higher frequencies due to the effects of parasitic capacitances. The most popular frequency range is from 10
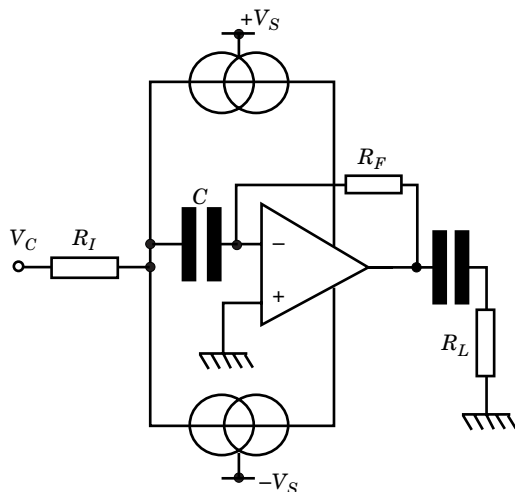
Figure 5. Supply current sensing current source, modified to stabilize the dc level at the output loop gain $A_L = A_0 \, R_I/R_L$.

kHz to 1000 kHz (16–21), although the system by Cusick (13) operates down to 100 Hz.

The current source design was improved to overcome an imbalance condition when an ac coupled load is used. The resistor R_F (100 MW) provides a dc negative feedback path: C (0.1 μF) has, relatively, a negligible impedance at 10 kHz, avoiding degradation of the ac performance of the supply-current-sensing current source (23).

Voltage Measurement

Electrode voltage signals are typically fed through coaxial cables with driven screens. A wide variety of instrumentation amplifiers with suitable bandwidth and low noise performance is now available. Early EIT voltage measurement designs incorporated analog multipliers to demodulate (synchronously detect) and measure the in-phase and quadrature components of the electrode voltages. The AD630 was frequently used. The output of the multiplier was low-pass filtered to obtain the impedance signal. There is necessarily a compromise between the amount of carrier left in the filtered signal and the response time of the filter to changes in the impedance. Digital demodulation was introduced by the RPI group and others, allowing better signal processing—removal of interference, signal averaging, narrower bandwidth, and adaptive filtering for different excitation signals. A nonuniform, oversampling method has been widely adopted: A digital signal generator is used to produce a reference sinusoidal waveform with, for instance, 256 samples per cycle. Therefore, 256 independent sampling points are available and can be used over 32 cycles to make 256 independent measurements from each of 32 electrode signals.

The duration of the sampling period for each electrode is roughly the whole measurement period, and hence the bandwidth is the reciprocal of the total period. Nonsynchronous noise will be filtered out. Synchronous noise will be minimized. The limitation with this method is the settling time after switching a new electrode signal to the ADC. Using video multiplexers, a sampling rate of 2.5 MHz is achievable; this gives a measurement period of 3 ms for each current pattern that is applied. Higher speeds are achievable if parallel

measurement circuits are used or if less than ideal measurement patterns are used.

This approach is applicable to both the pair-drive excitation method and multiple drive, since both require the establishment of multiple current patterns and concurrent voltage measurement for a full data set for the reconstruction of a single image. With 32 drive electrodes, 31 independent adjacent pair-drive combinations are possible; 31 independent trigonometric or optimal patterns can be set by multiple-drive systems.

APPLICATION AREAS

Medical Imaging

The first EIT equipment to become available commercially was the Sheffield Mark 1 2-D real-time difference imaging system (16). This system is able to show cardiac and respiratory cycles by displaying the difference in impedance between a reference measurement and the present measurement. The choice of reference can be end expiration for the best imaging of respiration or a point triggered from the electrocardiogram (ECG) waveform for best cardiovascular imaging.

More recently the Sheffield group has developed a 3-D system (24) by using eight planes of electrodes on a subject's chest. Differencing imaging is again employed, but the differences can be obtained by using multiple frequencies rather than temporal differences. Advanced image presentation techniques allow isometric viewing of the combined images from all planes. They have shown good resolution perpendicular to the electrode planes by imaging phantoms with targets clearly resolved on one plane and showing only faintly on the adjacent planes.

The leading North American Medical EIT group at RPI has achieved real-time imaging of human and dog chests using a multiple-drive system with 32 electrodes, delivering current and measuring voltage on the same electrodes. *Real time* refers to real-time data acquisition but slower off-line image reconstruction. Full-speed image replay is done later. The RPI group has been able to show cardiac and respiratory cycles as absolute impedance images and has performed physiological experiments with altered blood flow to the left and right lungs and imaged clear differences. The group's data also show concurrent rises in cardiac impedance with falls in lung impedance at the subject's heart rate.

Another static (or absolute) EIT system producing moving images has been developed at Oxford Brookes University. Real-time (as defined previously) imaging of human chests has shown cardiac and respiratory cycles, but poorer localization of the impedance changes than the similar RPI system. Principal component analysis applied to the data has been used to separate the cardiac-synchronous in-phase and (expected) antiphase heart and lung impedance changes.

Novel configurations of the Sheffield system have been developed by Smallwood (25) and by Kotre (26) in which a planar array of electrodes is applied to the front of the abdomen for monitoring gastric emptying. A modified back-projection reconstruction technique is used to localize the impedance changes close to the current-carrying electrodes, thereby allowing a simple method of imaging.

Other principal medical EIT applications include a system developed by Jossinet for investigating the detection of breast tumors, where absolute measurements are needed, and the

localization of epileptic foci and detection of brain ischemia (27).

Impedance Spectroscopy

In parallel with EIT imaging, many investigators have examined the impedance spectrum of tissue in vivo by placing electrodes in or close to supposed homogeneous regions for tissue characterization based on a lumped model for intra/extracellular current flow. In vitro measurements on isolated tissue have also been used to develop the Cole models. It is expected that when high-quality EIT data are available, it will be possible to detect pathological changes in tissues close to the skin surface, such as breast tumors, or unsuccessfully implanted kidneys.

Process Monitoring

Since the mid-1980s EIT techniques have been developed for process monitoring in industrial applications involving the identification of mixed components in pipelines, vessels, conveyers, and reactors. The excitation mode depends on whether the substances to be monitored and the container are conducting or insulating. Conducting substances in a conducting vessel are amenable to the techniques described for medical imaging as long as independent electrode sites are available on the container wall. A variant of this method is electromagnetic induction tomography, in which images are produced of eddy current loss in the materials. In the many cases where the container is insulating, electrical capacitance tomography (ECT) provides a rapid technique with a resolution comparable to EIT. Due to the large difference between water and oil permittivity (40 : 1), ECT is particularly appropriate to the oil industry. Dual ECT systems placed a short distance apart on a pipeline have been used to monitor flow by cross-correlating image features.

Imaging improvements have come from the placing of electrodes on stirrers or other accessible fixings within vessels, thereby overcoming the problem of poor resolution at the center of standard EIT images.

Geophysical Surveying and Archaeological Exploration

Electrical resistance tomography (ERT) can be used to image principally the water content of soil and porous rocks. The naturally occurring resistivity range is approximately 100 $\Omega \cdot m$ to 10,000 $\Omega \cdot m$; in experiments, changes up to 10% are seen when saline is added. Electrodes are inserted in deep boreholes, current is passed between them, and the resulting potentials are measured on either surface or other deep electrodes. The reconstruction methods have been adapted to consider the case where the electrodes are surrounded by conducting material. Three-dimensional imaging is best achieved by having deep voltage measurement electrodes, at the cost of getting them there. Similarly, anomalies in the resistance image can be of use in detecting buried archaeological features. In this context, time and current density are not constrained and will allow better resolution than in the medical context.

BIBLIOGRAPHY

1. R. E. Langer, On an inverse problem in differential equations, *Bull. Amer. Math. Soc.,* **39**: 814–820, 1933.

2. L. B. Slichter, The interpretation of the resistivity prospecting method for horizontal structures, *J. Appl. Phys.,* **4**: 307–322, 1933.

3. R. P. Henderson and J. G. Webster, An impedance camera for spatially specific measurement of the thorax, *IEEE Trans. Biomed. Eng.,* **25**: 250–254, 1978.

4. V. Isakov, *Inverse Problems for Partial Differential Equations,* New York: Springer-Verlag, 1998.

5. E. B. Curtis and J. A. Morrow, Determining the resistors in a network, *SIAM J. Appl. Math.,* **50**: 918–930, 1990.

6. Y. Colin de Verdiere, J. Gitler, and D. Vertigan, Planar electrical networks. 2, *Commentarii Mathematici Helvetici,* **71**: 144–167, 1996.

7. P. Ola and E. Somersalo, Electromagnetic inverse problems and generalized Sommerfeld potentials, *SIAM J. Appl. Math.,* **56** (4): 1129–1145, 1996.

8. H. Jain et al., Electrical impedance tomography of complex conductivity distributions with noncircular boundary, *IEEE Trans. Biomed. Eng.,* **44**: 1051–1060, 1997.

9. W. R. B. Lionheart, Boundary shape and electrical impedance tomography, *Inverse Problems,* **14**: 139–147, 1998.

10. K. Paulson, W. Breckon, and M. Pidcock, Electrode modeling in electrical-impedance tomography, *SIAM J. Appl. Math.,* **52**: 1012–1022, 1992.

11. W. R. Breckon, *Image reconstruction in electrical impedance tomography,* Ph.D. thesis, Oxford Polytechnic, 1990.

12. M. Cheney and D. Isaacson, Distinguishability in impedance imaging, *IEEE Trans. Biomed. Eng.,* **39**: 852–860, 1992.

13. B. M. Eyuboglu and T. C. Pilkington, Comments on distinguishability in electrical-impedance tomography, *IEEE Trans. Biomed. Eng.,* **41**: 505, 1994.

14. B. Rigaud, J-P. Morucci, and N. Chauveau, Bioelectrical impedance techniques in medicine, *Crit. Rev. Biomed. Eng.,* **24** (4–6): 257–351, 1996.

15. R. D. Cook et al., ACT3: A high-speed, high-precision electrical impedance tomograph, *IEEE Trans. Biomed. Eng.,* **41**: 713–722, 1994.

16. D. C. Barber, B. H. Brown, and I. L. Freeston, Imaging spatial distributions of resistivity using applied potential tomography, *Electron. Lett.,* **19**: 933–935, 1983.

17. P. J. Riu et al., Multifrequency static imaging in electrical-impedance tomography. 1. Intrumentation requirements, *Med. Biol. Eng. Comput.,* **33**: 784–792, 1995.

18. H. Griffiths and J. Jossinet, Bioelectrical spectroscopy from multi-frequency EIT, *Physiol. Meas.,* **15** (Suppl. 2A): A59–63, 1994.

19. J. Jossinet, C. Trillaud, and E. T. McAdams, A distributed front-end tomograph for high-frequency electrical impedance imaging, *Proc. 8th ICEBI,* Kuopio, Finland, 1992.

20. P. M. Record, Single-plane multifrequency electrical impedance instrumentation, *Physiol. Meas.,* **15** (Suppl. 2A): A29–35, 1994.

21. Q. Zhu et al., An adaptive current tomography using voltage sources, *IEEE Trans. Biomed. Eng.,* **40**: 163–168, 1993.

22. G. Cusick et al., A system for impedance imaging epilepsy in ambulatory human subjects, *Innov. Tech. Biol. Med.,* **15** (1): 33–39, 1994.

23. C. W. Denyer et al., A high-output impedance current source, *Physiol. Meas.,* **15**: A79–A82, 1994.

24. P. Metherall et al., Three-dimensional electrical-impedance tomography, *Nature,* **380**: 509–512, 1996.

25. R H. Smallwood, Y. F. Mangnall, and A. D. Leathard, Transport of gastric contents, *Physiol. Meas.,* **15**: A175–A188, 1994.

26. C. J. Kotre, Subsurface electrical-impedance imaging using orthogonal linear electrode arrays, *IEEE Proc.-Sci. Meas. Tech.,* **143**: 41–46, 1996.

27. D. S. Holder, Electrical-impedance tomography with cortical or scalp electrodes during global cerebral-ischemia in the anesthetized rat, *Clin. Phys. Physiol. Meas.,* **13**: 87–98, 1992.

CHRISTOPHER N. MCLEOD

WILLIAM R. B. LIONHEART
Oxford Brookes University

ELECTRICITY METERING.   See WATTHOUR METERS.
ELECTRICITY, STATIC.   See STATIC ELECTRIFICATION.